Wei *et al. Advances in Aerodynamics* (2023) 5:25
https://doi.org/10.1186/s42774-023-00156-y

Advances in Aerodynamics

RESEARCH

Open Access

Adaptive wave-particle decomposition in UGKWP method for high-speed flow simulations

Yufeng Wei[1], Junzhe Cao[2], Xing Ji[3] and Kun Xu[1,4,5*]

*Correspondence: makxu@ust.hk

[1] Department of Mathematics, Hong Kong University of Science and Technology, Hong Kong, China
[2] School of Aeronautics, Northwestern Polytechnical University, Xi'an 710072, China
[3] Shaanxi Key Laboratory of Environment and Control for Flight Vehicle, Xi'an Jiaotong University, Xi'an, 710049, China
[4] Department of Mechanical and Aerospace Engineering, Hong Kong University of Science and Technology, Hong Kong, China
[5] HKUST Shenzhen Research Institute, Shenzhen 518057, China

Abstract

With wave-particle decomposition, a unified gas-kinetic wave-particle (UGKWP) method has been developed for multiscale flow simulations. With the variation of the cell Knudsen number, the UGKWP method captures the transport process in all flow regimes without the kinetic solver's constraint on the numerical mesh size and time step being determined by the kinetic particle mean free path and particle collision time. In the current UGKWP method, the cell Knudsen number, which is defined as the ratio of particle collision time to numerical time step, is used to distribute the components in the wave-particle decomposition. The adaptation of particles in the UGKWP method is mainly for the capturing of the non-equilibrium transport. In this aspect, the cell Knudsen number alone is not enough to identify the non-equilibrium state. For example, in the equilibrium flow regime with a Maxwellian distribution function, even at a large cell Knudsen number, the flow evolution can be still modelled by the Navier-Stokes solver. More specifically, in the near space environment both the hypersonic flow around a space vehicle and the plume flow from a satellite nozzle will encounter a far field rarefied equilibrium flow in a large computational domain. In the background dilute equilibrium region, the large particle collision time and a uniform small numerical time step can result in a large local cell Knudsen number and make the UGKWP method track a huge number of particles for the far field background flow in the original approach. But, in this region the analytical wave representation can be legitimately used in the UGKWP method to capture the nearly equilibrium flow evolution. Therefore, to further improve the efficiency of the UGKWP method for multiscale flow simulations, an adaptive UGKWP (AUGKWP) method is developed with the introduction of an additional local flow variable gradient-dependent Knudsen number. As a result, the wave-particle decomposition in the UGKWP method is determined by both the cell and gradient Knudsen numbers, and the use of particles in the UGKWP method is solely to capture the non-equilibrium flow transport. The current AUGKWP method becomes much more efficient than the previous one with the cell Knudsen number only in the determination of wave-particle composition. Many numerical tests, including Sod shock tube, normal shock structure, hypersonic flow around cylinder, flow around reentry capsule, and an unsteady nozzle plume flow, have been conducted to validate the accuracy and efficiency of the AUGKWP method. Compared with the original UGKWP method, the AUGKWP method achieves the same

Springer Open

© The Author(s) 2023. **Open Access** This article is licensed under a Creative Commons Attribution 4.0 International License, which permits use, sharing, adaptation, distribution and reproduction in any medium or format, as long as you give appropriate credit to the original author(s) and the source, provide a link to the Creative Commons licence, and indicate if changes were made. The images or other third party material in this article are included in the article's Creative Commons licence, unless indicated otherwise in a credit line to the material. If material is not included in the article's Creative Commons licence and your intended use is not permitted by statutory regulation or exceeds the permitted use, you will need to obtain permission directly from the copyright holder. To view a copy of this licence, visit http://creativecommons.org/licenses/by/4.0/.

accuracy, but has advantages in memory reduction and computational efficiency in the simulation for flows with the co-existing of multiple regimes.

Keywords: Adaptive wave-particle decomposition, Multiscale modeling, Acceleration method, Non-equilibrium transport

1 Introduction

Around a high-speed flying vehicle with complex irregular large-scale configurations in near-space flight surrounding, the highly compressed gas nearby the leading edge and the strong expansion wave around the leeward zone cover multiflow zone mixed flows with huge pressure and density differences due to the influence of viscosity and adverse pressure gradients at the same flying altitude [1]. In the control system of a moving satellite, the flow expansion inside a nozzle can undergo a rapid and unstable transition from continuum to free-molecule flow as the local Knudsen number varies by an order of magnitude of ten. This transition occurs as the high-pressure gas inside the nozzle expands into the background vacuum. Multiscale flows involve a large variation of Knudsen number and significant changes of the degrees of freedom in the description of flow physics. In aerospace applications, an accurate and efficient multiscale method with the capability of simulating both continuum and rarefied flows is of great importance [2].

The Boltzmann equation is the fundamental governing equation for rarefied gas dynamics. Theoretically, it can capture multiscale flow physics in all Knudsen regimes, with the enforcement to the modeling scales of the Boltzmann equation, such as the particle mean free path and mean collision time. For a non-equilibrium flow, there are mainly two kinds of numerical methods to solve the Boltzmann equation, i.e., the stochastic particle method and the deterministic discrete velocity method. The stochastic methods employ discrete particles to simulate the statistical behavior of molecular gas dynamics [1, 3–11]. This kind of Lagrangian-type scheme achieves high computational efficiency and robustness in rarefied flow simulation, especially for hypersonic flow. However, it suffers from statistical noise in the low-speed flow simulation due to its intrinsic stochastic nature. Meanwhile, in the near continuum flow regime, the particle method becomes very expensive due to the requirement of small cell size and time step in the computational space and the tracking of a large number of particles with intensive collisions. The deterministic approaches use discrete particle velocity space to solve the kinetic equation and naturally obtain accurate solutions without statistical noise [12–25]. At the same time, the deterministic method can achieve high efficiency using numerical acceleration techniques, such as implicit algorithms [14, 13, 26–29], memory reduction techniques [24], adaptive refinement methods [30], and fast evaluation of the Boltzmann collision term [31, 32]. Asymptotic preserving (AP) schemes [33, 34] and unified preserving (UP) schemes [35] can be developed to release the stiffness of the collision term at the small Knudsen number case. However, for most AP schemes only the Euler solution in the hydrodynamic limit is recovered, where the NS limit can be obtained in the AP schemes. Additionally, for hypersonic and rarefied flows, the deterministic methods have to use a gigantic number of grid points in the particle velocity space to cover a large variation of particle velocity and resolve the non-equilibrium distribution. The three-dimensional hypersonic flow calculation can be hardly conducted

due to the huge memory consumption and computational cost. Moreover, for both stochastic and deterministic methods, with the operator-splitting treatment of particle free transport and instant collision, a numerical dissipation proportional to the time step is usually unavoidable. Therefore, the mesh size and the time step in both the traditional particle method, such as DSMC, and the deterministic DVM method, are required to be less than the particle mean free path and collision time, to avoid the physical dissipation being overwhelmingly taken over by the numerical ones, especially in the continuum flow regime, such as the laminar boundary layer computation at a high Reynolds number [36]. In order to remove the constraints on the mesh size and time step in the continuum flow regime, the unified gas-kinetic scheme (UGKS) and discrete UGKS (DUGKS) with the coupled particle transport and collision in the flux evaluation have been constructed successfully [18, 29, 37]. At the same time, the multiscale particle methods have been constructed as well [38, 39].

Combining the advantages of the deterministic and the stochastic methods, a unified gas-kinetic wave-particle (UGKWP) method [40, 41] has been proposed under the UGKS framework [2, 42], as well as simplified versions [43, 44]. The method has included molecular rotation and vibration [45, 46], and has been extended to other multiscale transports, such as radiation, plasma, and multiphase flow [47–49]. Taking advantage of the evolution solution of the kinetic model equation [50] in the scheme construction, the UGKWP method can capture the flow physics in all flow regimes and release the restrictions on the mesh size and time step which are previously imposed on the kinetic solvers. In the rarefied flow region with a large cell Knudsen number, the UGKWP method becomes a particle method for the capturing of peculiar gas distribution function. In the continuum region with a small cell Knudsen number, the UGKWP method gets back to a hydrodynamic flow solver, where the gas-kinetic scheme (GKS) for the Navier-Stokes solution [51] is fully recovered. Different from domain decomposition methods with buffer zones, the UGKWP method employs wave-particle decomposition in each cell with a unified treatment in the whole computational domain. The essential criterion used in the UGKWP method to identify different flow regimes is according to the cell Knudsen number $Kn_c = \tau/\Delta t$, where τ is the local particle collision time and Δt is the numerical time step. Naturally the cell Knudsen number controls the weights in the wave-particle decomposition. However, besides identifying the real non-equilibrium flow region, the large cell Knudsen number also picks up a dilute equilibrium state as the rarefied regime and uses particles to simulate the background equilibrium flow evolution. For example, the far field of hypersonic flow around a space vehicle is usually in an equilibrium state with a Maxwellian distribution, and the cell Knudsen number in the background equilibrium state is large. The large cell Knudsen number will increase the weight of particles while in reality the analytical wave can be faithfully used in this region. In this paper, besides the cell Knudsen number, a new parameter for identifying the local non-equilibrium state will be introduced and added to the previous criteria for wave-particle decomposition. As a result, an adaptive unified gas-kinetic wave-particle method (AUGKWP) will be constructed with a clear identification of the non-equilibrium region. The new method will avoid using particles to the background dilute equilibrium region and further improve the computational efficiency of the UGKWP method.

The paper is organized as follows. Since the UGKWP method is an enhanced version of the solely particle-based unified gas-kinetic particle (UGKP) method by employing both wave and particle compositions, the UGKP method will be introduced first in Section 2. The UGKWP method will be discussed in Section 3. Then the adaptive UGKWP method by mainly concentrating particle distribution to the non-equilibrium flow region will be presented in Section 4. Numerical validation of the current method will be carried out in Section 5 and a conclusion will be drawn in Section 6.

2 Unified gas-kinetic particle method

2.1 General framework

The unified gas-kinetic particle (UGKP) method is a particle implementation of the UGKS under the finite volume framework, where the discrete particles are employed to describe the non-equilibrium gas distribution function, and the evolution of particles recovers the multiscale nature in different flow regimes. The kinetic equation with BGK relaxation model is

$$\frac{\partial f}{\partial t} + \boldsymbol{u} \cdot \frac{\partial f}{\partial \boldsymbol{r}} = \frac{g - f}{\tau}, \tag{1}$$

where the equilibrium state g is the Maxwellian distribution function,

$$g = \rho \left(\frac{\lambda}{\pi} \right)^{\frac{d}{2}} e^{-\lambda \boldsymbol{c}^2},$$

where d is the degrees of freedom, and λ is related to the temperature T by $\lambda = m_0/2k_B T$. Here, m_0 and k_B are the molecular mass and Boltzmann constant, respectively. $\boldsymbol{c} = \boldsymbol{u} - \boldsymbol{U}$ denotes the peculiar velocity. Along the characteristic line, the integral solution of the kinetic model equation gives

$$f(\boldsymbol{r}, t) = \frac{1}{\tau} \int_0^t e^{-(t-t')/\tau} g(\boldsymbol{r}', t') \mathrm{d}t' + e^{-t/\tau} f_0(\boldsymbol{r} - \boldsymbol{u}t), \tag{2}$$

where $f_0(\boldsymbol{r})$ is the initial distribution function at the beginning of each step t_n, and $g(\boldsymbol{r}, t)$ is the equilibrium state distributed in space and time around $\boldsymbol{r}$ and t. The integral solution describes an evolution process from the non-equilibrium state to the equilibrium state through particle collisions.

In the UGKS, with the expansion of the initial distribution function and the equilibrium state

$$\begin{aligned} f_0(\boldsymbol{r}) =& f_0 + \boldsymbol{r} \cdot \frac{\partial f}{\partial \boldsymbol{r}}, \\ g(\boldsymbol{r}, t) =& g_0 + \boldsymbol{r} \cdot \frac{\partial g}{\partial \boldsymbol{r}} + \frac{\partial g}{\partial t} t, \end{aligned} \tag{3}$$

the second-order accurate flux for macroscopic flow variables across cell interface ij can be constructed from the integral solution,

$$
\begin{aligned}
\boldsymbol{F}_{ij} =& \frac{1}{\Delta t}\int_0^{\Delta t}\int \boldsymbol{u}\cdot\boldsymbol{n}_{ij} f_{ij}(t)\boldsymbol{\psi}\,\mathrm{d}\boldsymbol{\Xi}\,\mathrm{d}t \\
=& \int \boldsymbol{u}\cdot\boldsymbol{n}_{ij}\left[C_1 g_0 + C_2\boldsymbol{u}\cdot\frac{\partial g}{\partial \boldsymbol{r}} + C_3\frac{\partial g}{\partial t}\right]\boldsymbol{\psi}\,\mathrm{d}\boldsymbol{\Xi} + \int \boldsymbol{u}\cdot\boldsymbol{n}_{ij}\left[C_4 f_0 + C_5\boldsymbol{u}\cdot\frac{\partial f}{\partial \boldsymbol{r}}\right]\boldsymbol{\psi}\,\mathrm{d}\boldsymbol{\Xi} \\
=& \boldsymbol{F}_{ij}^{eq} + \boldsymbol{F}_{ij}^{fr},
\end{aligned}
\tag{4}
$$

where $\boldsymbol{n}_{ij}$ is the normal vector of the cell interface, and

$$
\boldsymbol{\psi} = \left(1, \boldsymbol{u}, \frac{1}{2}\boldsymbol{u}^2\right)^T.
$$

$\boldsymbol{F}_{ij}^{fr}$ and $\boldsymbol{F}_{ij}^{eq}$ are the macroscopic fluxes from the free transport and collision processes, respectively. The integrated time coefficients are

$$
\begin{aligned}
C_1 =& 1 - \frac{\tau}{\Delta t}\left(1 - e^{-\Delta t/\tau}\right), \\
C_2 =& -\tau + \frac{2\tau^2}{\Delta t} - e^{-\Delta t/\tau}\left(\frac{2\tau^2}{\Delta t} + \tau\right), \\
C_3 =& \frac{1}{2}\Delta t - \tau + \frac{\tau^2}{\Delta t}\left(1 - e^{-\Delta t/\tau}\right), \\
C_4 =& \frac{\tau}{\Delta t}\left(1 - e^{-\Delta t/\tau}\right), \\
C_5 =& \tau e^{-\Delta t/\tau} - \frac{\tau^2}{\Delta t}(1 - e^{-\Delta t/\tau}).
\end{aligned}
$$

The UGKS updates both the gas distribution function and macroscopic flow variables under a finite volume framework. In the UGKP method, the particle will be used to follow the evolution of the gas distribution function directly and keep the finite volume version for the updates of macroscopic flow variables. On the microscopic scale, the particle evolution follows the evolution solution in Eq. (2), where the particle free transport and collision will be taken into account. On the macroscopic scale, the fluxes across the cell interface for the updates of macroscopic flow variables inside each control volume are evaluated by Eq. (4).

Denote a simulation particle as $P_k(m_k, \boldsymbol{r}_k, \boldsymbol{u}_k)$, which represents a package of real gas molecules at location $\boldsymbol{r}_k$ with particle mass m_k and microscopic velocity $\boldsymbol{u}_k$. According to the evolution solution, the cumulative distribution function of particle's collision is

$$
\mathcal{G}(t) = 1 - \exp(-t/\tau),
$$

then the free transport time of a particle within one time step Δt will be

$$
t_f = \min(-\tau \ln \eta, \Delta t),
\tag{5}
$$

where η is a random number uniformly distributed in (0, 1). In a numerical time step from t^n to t^{n+1}, according to the free transport time t_f, the simulation particles can be categorized into collisionless particles ($t_f = \Delta t$) and collisional particles ($t_f < \Delta t$).

In the free transport process, i.e., $t < t_f$, no collisions will happen, and the particles move freely and carry the initial information. The trajectory of particle P_k could be fully tracked by

$$\boldsymbol{x}_k = \boldsymbol{x}_k^n + \boldsymbol{u}_k t_{f,k}. \tag{6}$$

During the free transport process, the effective net flux across interfaces of cell i can be evaluated by

$$\boldsymbol{W}_i^{fr} = \frac{1}{\Delta t}\left(\sum_{\boldsymbol{x}_k \in \Omega_i} \boldsymbol{\phi}_k - \sum_{\boldsymbol{x}_k^n \in \Omega_i} \boldsymbol{\phi}_k\right), \tag{7}$$

where $\boldsymbol{\phi}_k = (m_k, m_k \boldsymbol{u}_k, \frac{1}{2} m_k \boldsymbol{u}_k^2)^T$. The free transport flux $\boldsymbol{F}_{ij}^{fr}$ in Eq. (4) has been recovered by the particles' movement.

In the free transport process, the particle during the time interval $(0, t_f)$ is fully tracked. The collisionless particles with $t_f = \Delta t$ are kept at the end of the time step. The collisional particles with $t_f < \Delta t$ would encounter collisions at t_f and they are only tracked up to this moment. Then, all collisional particles are removed, but their accumulated mass, momentum, and energy inside each cell can be still updated through the evolution of macroscopic variables. These collisional particles can be re-sampled from the updated macroscopic variables at the beginning of the next time step from the equilibrium state if needed.

The equilibrium flux $\boldsymbol{F}_{ij}^{eq}$ in Eq. (4) contains three terms, i.e., g, $\partial_{\boldsymbol{r}} g$ and $\partial_t g$, which are only related to the equilibrium states and can be fully determined by the macroscopic flow variables. Once the Maxwellian distribution and its derivatives around the cell interface are determined, the equilibrium flux $\boldsymbol{F}_{ij}^{eq}$ can be obtained by

$$\boldsymbol{F}_{ij}^{eq} = \int \boldsymbol{u} \cdot \boldsymbol{n}_{ij} \left[C_1 g_0 + C_2 \boldsymbol{u} \cdot \frac{\partial g}{\partial \boldsymbol{r}} + C_3 \frac{\partial g}{\partial t}\right] \boldsymbol{\psi} \, \mathrm{d}\boldsymbol{\Xi}. \tag{8}$$

The macroscopic variables for the determination of the equilibrium state g_0 at cell interface ij are coming from the colliding particles from both sides of the cell interface,

$$\boldsymbol{W}_{ij} = \int \left[g^l H[\bar{u}_{ij}] + g^r (1 - H[\bar{u}_{ij}])\right] \boldsymbol{\psi} \, \mathrm{d}\boldsymbol{\Xi},$$

where $\bar{u}_{ij} = \boldsymbol{u} \cdot \boldsymbol{n}_{ij}$ and $H[x]$ is the Heaviside function. The gradient of the equilibrium state is obtained from the gradient of macroscopic flow variables $\partial \boldsymbol{W}_{ij}/\partial \boldsymbol{r}$. In this study, the spatial reconstruction of macroscopic flow variables is carried out by the least-square method with Venkatakrishnan limiter [52]. As to the temporal gradient, the compatibility condition on Eq. (1)

$$\int (g - f) \boldsymbol{\psi} \, \mathrm{d}\Xi = 0$$

is employed to give

$$\frac{\partial \boldsymbol{W}_{ij}}{\partial t} = -\int \boldsymbol{u} \cdot \frac{\partial g}{\partial \boldsymbol{r}} \boldsymbol{\psi} \, \mathrm{d}\boldsymbol{\Xi}.$$

Correspondingly, the temporal gradient of the equilibrium state $\partial_t g$ can be evaluated from the above $\partial \boldsymbol{W}_{ij}/\partial t$. With g_0, $\partial_{\boldsymbol{r}} g$ and $\partial_t g$, the equilibrium flux $\boldsymbol{F}_{ij}^{eq}$ can be fully determined.

2.2 Updates of macroscopic variables and discrete particles

Under the finite volume framework, according to the conservation law, the updates of macroscopic variables can be written as

$$\boldsymbol{W}_i^{n+1} = \boldsymbol{W}_i^n - \frac{\Delta t}{\Omega_i} \sum_{j \in N(i)} \boldsymbol{F}_{ij}^{eq} \mathcal{A}_{ij} + \frac{\Delta t}{\Omega_i} \boldsymbol{W}_i^{fr}, \tag{9}$$

where $\boldsymbol{W}_i^{fr}$ is the net free streaming flow of cell i calculated by particle tracking in the free transport process in Eq. (7), and the equilibrium flux $\boldsymbol{F}_{ij}^{eq}$ is evaluated from macroscopic flow variables and their gradients in Eq. (8).

Substituting Eq. (3) into the integral solution Eq. (2) of the kinetic model equation, the time evolution of the distribution function along the characteristic line is

$$f(\boldsymbol{r}, t) = (1 - e^{-t/\tau}) g(\boldsymbol{r}', t') + e^{-t/\tau} f_0(\boldsymbol{r} - \boldsymbol{u}t),$$

where

$$\boldsymbol{r}' = \boldsymbol{u}\left(\frac{te^{-t/\tau}}{1 - e^{-t/\tau}} - \tau\right), \quad t' = \left(\frac{te^{-t/\tau}}{1 - e^{-t/\tau}} - \tau\right) + t.$$

It indicates that the collisional particles will follow the near-equilibrium state $g(\boldsymbol{r}', t')$ after collision within the time step $t_f < \Delta t$. With the updated macroscopic flow variables, these untracked collisional particles within the time $t \in (t_f, \Delta t)$ can be re-sampled from the hydro-particle macroscopic quantities,

$$\boldsymbol{W}_i^{h,n+1} = \boldsymbol{W}_i^{n+1} - \boldsymbol{W}_i^{p,n+1} = \boldsymbol{W}_i^{n+1} - \frac{1}{\Omega_i} \sum_{x_k^{n+1} \in \Omega_i} \boldsymbol{\phi}_k, \tag{10}$$

where $\boldsymbol{W}_i^{p,n+1}$ is from the collisionless particles remaining in cell i. With the macroscopic quantities and the form of the equilibrium state g, the corresponding particles can be generated. Details of sampling from a given distribution function are provided in [41].

The free transport and collision processes for both microscopic discrete particles and macroscopic flow variables have been described above. Here, we give a summary of the procedures of the UGKP method. Following the illustration in [41], the algorithm of the UGKP method for diatomic gases with molecular translation, rotation and vibration can be summarized as follows.

Step 1 For the initialization, sample particles from the given initial conditions as shown in Fig. 1(a).

Step 2 Generate the free transport time t_f for each particle by Eq. (5), and classify the particles into collisionless particles (white circles in Fig. 1(b)) and collisional ones (solid circles in Fig. 1(b)). Stream the particles for the free transport time by Eq. (6), and evaluate the net free streaming flow $\boldsymbol{W}_i^{fr}$ by Eq. (7).

Step 3 Reconstruct macroscopic flow variables and compute the equilibrium flux $\boldsymbol{F}_{ij}^{eq}$ by Eq. (8).

Step 4 Update the macroscopic flow variables $\boldsymbol{W}_i$ by Eq. (9). Obtain the updated hydro-particle macroscopic quantities of collisional particles $\boldsymbol{W}_i^h$ by extracting the macro-

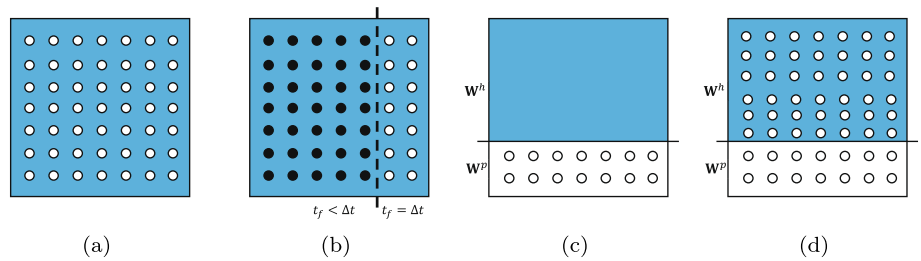

Fig. 1 Diagram to illustrate the composition of the particles during time evolution in the UGKP method. (**a**) Initial field, (**b**) classification of the collisionless particles (white circles) and collisional particles (solid circles) according to the free transport time t_f, (**c**) update solution at the macroscopic level, and (**d**) update solution at the microscopic level

quantities of collisionless particles $\boldsymbol{W}_i^p$ from the total flow variables $\boldsymbol{W}_i$ in Eq. (10) as shown in Fig. 1(c).

Step 5 Delete the collisional particles at t_f and re-sample these particles from the updated hydro-particle macroscopic variables $\boldsymbol{W}_i^h$ as shown in Fig. 1(d), which becomes the initial state in Fig. 1(a) at the beginning of the next time step.

Step 6 Go to Step 2. Continue time step evolution until the finishing time.

3 Unified gas-kinetic wave-particle method

In the UGKP method, based on the updated hydro-particle macroscopic variables $\boldsymbol{W}_i^h$ of collisional particles, these particles will be re-sampled from the equilibrium state at the beginning of the next time step. However, some of these re-sampled particles will get collision in the next time step and get eliminated again. Therefore, in the unified gas-kinetic wave-particle (UGKWP) method, only free transport particles in the next time step will be re-sampled from $\boldsymbol{W}_i^h$. In the continuum regime at a very small Knudsen number, it is possible that no free particles will get re-sampled.

The collisionless particles with $t_f = \Delta t$ will be sampled from $\boldsymbol{W}_i^h$. According to the integral solution, the collisionless particles will take a fraction of $\boldsymbol{W}_i^h$ by the amount,

$$\boldsymbol{W}_i^{hp} = e^{\frac{-\Delta t}{\tau}} \boldsymbol{W}_i^h. \tag{11}$$

As shown in Fig. 2, there is no need to sample these collisional particles from the hydrodynamic portion with macroscopic variables $(\boldsymbol{W}_i^h - \boldsymbol{W}_i^{hp})$. The free transport flux from these un-sampled collisional particles can be evaluated analytically,

$$\boldsymbol{F}_{ij}^{fr,h} = \int \boldsymbol{u} \cdot \boldsymbol{n}_{ij} \left[C_4' g_0 + C_5' \boldsymbol{u} \cdot \frac{\partial g}{\partial \boldsymbol{r}} \right] \boldsymbol{\psi} \, \mathrm{d}\boldsymbol{\Xi}, \tag{12}$$

where

$$C_4' = \frac{\tau}{\Delta t}\left(1 - e^{-\Delta t/\tau}\right) - e^{-\Delta t/\tau},$$
$$C_5' = \tau e^{-\Delta t/\tau} - \frac{\tau^2}{\Delta t}(1 - e^{-\Delta t/\tau}) + \frac{1}{2}\Delta t e^{-\Delta t/\tau}.$$

Then, the update of macroscopic flow variables in the UGKWP method becomes

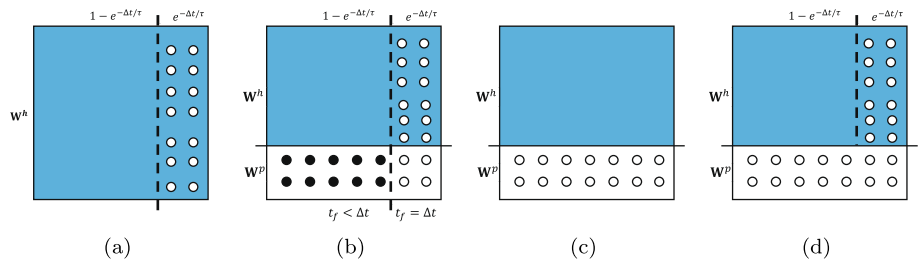

Fig. 2 Diagram to illustrate the composition of the particles during time evolution in the UGKWP method. (**a**) Initial field, (**b**) classification of the collisionless and collisional particles for $\boldsymbol{W}_i^p$, (**c**) update on the macroscopic level, and (**d**) update on the microscopic level

$$\boldsymbol{W}_i^{n+1} = \boldsymbol{W}_i^n - \frac{\Delta t}{\Omega_i}\sum_{j\in N(i)} \boldsymbol{F}_{ij}^{eq}\mathcal{A}_{ij} - \frac{\Delta t}{\Omega_i}\sum_{j\in N(i)} \boldsymbol{F}_{ij}^{fr,h}\mathcal{A}_{ij} + \frac{\Delta t}{\Omega_i}\boldsymbol{W}_i^{fr,p} + \boldsymbol{S}_i. \tag{13}$$

The algorithm of the UGKWP method for diatomic gases can be summarized as follows.

Step 1 For the initialization, sample collisionless particles from $\boldsymbol{W}_i^{hp}$ with $t_f = \Delta t$ as shown in Fig. 2(a). For the first step, $\boldsymbol{W}_i^h = \boldsymbol{W}_i^{n=0}$.

Step 2 Generate the free transport time t_f by Eq. (5) for the remaining particles from the previous step evolution with total amount $\boldsymbol{W}_i^p$, and classify the particles into collisionless particles (white circles in Fig. 2(b)) and collisional ones (solid circles in Fig. 2(b)). Stream the particles for the free transport time by Eq. (6), and evaluate the net free streaming flow $\boldsymbol{W}_i^{fr}$ by Eq. (7).

Step 3 Reconstruct macroscopic flow variables and compute the free transport flux of collisional particles $\boldsymbol{F}_{ij}^{fr,h}$ by Eq. (12) and the equilibrium flux $\boldsymbol{F}_{ij}^{eq}$ by Eq. (8).

Step 4 Update the macroscopic flow variables $\boldsymbol{W}_i$ by Eq. (13). Obtain the updated macroscopic quantities for collisional particles $\boldsymbol{W}_i^h$ by extracting the macro-quantities of collisionless particles $\boldsymbol{W}_i^p$ from the total flow variables $\boldsymbol{W}_i$ in Eq. (10) as shown in Fig. 2(c).

Step 5 Delete the collisional particles at t_f ($t_f < \Delta t$). Re-sample the collisionless particles from $\boldsymbol{W}_i^{hp}$ with $t_f = \Delta t$ at the beginning of the next time step, as shown in Fig. 2(d).

Step 6 Go to Step 2. Continue time evolution until the output time.

The UGKP method uses particles to represent the gas distribution function. However, the UGKWP method adopts a hybrid formulation of wave and particles to recover the gas distribution function. Within the time step, the evolution of wave part for the collisional particles ($t_f < \Delta t$) can be described analytically by the time accurate solution of macroscopic flow variables without sampling these particles explicitly. The evolution of the remaining particles will track the non-equilibrium effect through particle free transport. In the rarefied flow regime, the UGKWP method is dominated by particle evolution, which results in a particle method. While in the continuum regime, the UGKWP method is mainly about the evolution of macroscopic variables, and the scheme becomes

a hydrodynamic NS solver, such as the so-called gas-kinetic scheme (GKS) [51]. Therefore, the UGKWP method achieves much better computational efficiency and lower memory consumption than the pure particle method UGKP.

However, the weights of wave and particles in the current UGKWP method are controlled by the cell Knudsen number $\tau/\Delta t$. The total mass fraction of particles is proportional to $e^{-\Delta t/\tau}\boldsymbol{W}$. There are still weaknesses in the above formulation. For example, even in the continuum flow regime, if a small time step Δt is used, the particles will emerge automatically in the flow evolution. At the same time, for a dilute background equilibrium distribution in the near space environment with a large particle collision time τ, the UGKWP method will use the particles to capture the background equilibrium flow evolution. Therefore, besides the cell Knudsen number, in order to use particles to really capture the evolution of the non-equilibrium state, another parameter has to be designed as well in the determination of the distributions between wave and particle in the UGKWP method.

4 Adaptive unified gas-kinetic wave-particle method

For the UGKWP method, the evaluation of flow regimes depends on the cell Knudsen number. However, this criterion cannot capture the real non-equilibrium regime, especially for the rarefied undisturbed equilibrium flow and the flow simulation with a very small numerical time step for high resolution. Even in the equilibrium regime, the large particle collision time and the small time step can give a large cell Knudsen number for particle generation. Theoretically, the analytical wave can be used in those equilibrium regimes. Besides the cell Knudsen number, the adaptive unified gas-kinetic wave-particle (AUGKWP) method will be developed by introducing another parameter to identify the real non-equilibrium region for the generation of particles. This parameter is a gradient-length related local Knudsen number Kn_{Gll}. In other words, the analytical wave will take effect as well when Kn_{Gll} is small. Therefore, the portion from the macroscopic flow variables to sample particles becomes

$$\boldsymbol{W}_i^{hp} = e^{\frac{-\Delta t}{\tau}}\eta(Kn_{Gll})\boldsymbol{W}_i^h,$$

where

$$\eta(Kn_{Gll}) = \frac{1}{2}\left[\tanh\left(\frac{Kn_{Gll}/Kn_{ref} - 1}{Kn_{ref}}\right) + 1\right],$$

and the gradient-length local Knudsen number is defined by

$$Kn_{Gll} = \frac{l_{mfp}}{\rho/|\nabla\rho|},$$

where l_{mfp} is the local mean free path. The reference Knudsen number Kn_{ref} is included as a critical value to evaluate the equilibrium and non-equilibrium regimes and thus directly control the wave-particle decomposition in each control volume. Then, the analytical free transport flux from un-sampled particles is amended as

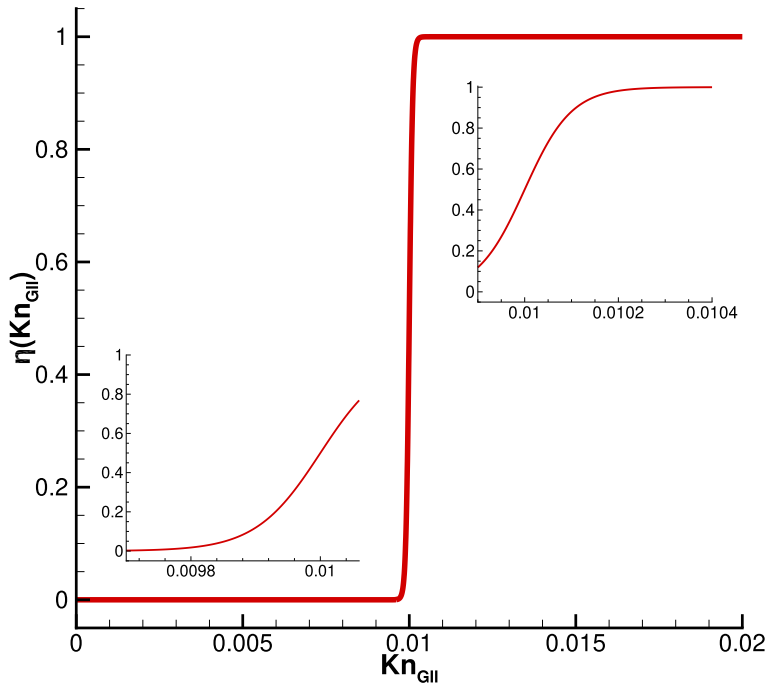

Fig. 3 The function $\eta(Kn_{Gll})$ at a reference Knudsen number $Kn_{ref} = 0.01$

$$\boldsymbol{F}_{ij}^{fr,h} = \int \boldsymbol{u} \cdot \boldsymbol{n}_{ij} \left[C_4^{Kn_{Gll}} g_0 + C_5^{Kn_{Gll}} \boldsymbol{u} \cdot \frac{\partial g}{\partial \boldsymbol{r}} \right] \boldsymbol{\psi} \, \mathrm{d}\boldsymbol{\Xi},$$

where

$$\begin{aligned} C_4^{Kn_{Gll}} =& \frac{\tau}{\Delta t}\left(1 - e^{-\Delta t/\tau}\right) - e^{-\Delta t/\tau} \eta(Kn_{Gll}), \\ C_5^{Kn_{Gll}} =& \tau e^{-\Delta t/\tau} - \frac{\tau^2}{\Delta t}(1 - e^{-\Delta t/\tau}) + \frac{1}{2}\Delta t e^{-\Delta t/\tau} \eta(Kn_{Gll}). \end{aligned}$$

In the AUGKWP method, a hyperbolic tangent function shown in Fig. 3 is used in the determination of the wave-particle decomposition due to its boundness, smoothness, and convexity. Its boundness ensures a natural transition without further restriction, and the smoothness avoids the oscillation in the transition regime. Its convexity satisfies the expectation for sampling particles with a slow rate of change in the continuum regime and a large rate otherwise. Moreover, the reference Knudsen number Kn_{ref} can be straightforwardly added in this function as a value to distinguish the flow regime, and can be conveniently adjusted according to the flow condition.

Figure 4 illustrates the wave-particle decomposition in the AUGKWP method in the limit of free molecular and continuum flow regimes. Different from domain decomposition methods, the AUGKWP method employs an adaptive wave-particle formulation in each control volume with a unified treatment when the reference Knudsen number is fixed. In the AUGKWP method, the adjustment of the reference Knudsen number influences the weights of wave and particles in each cell, instead of identifying different

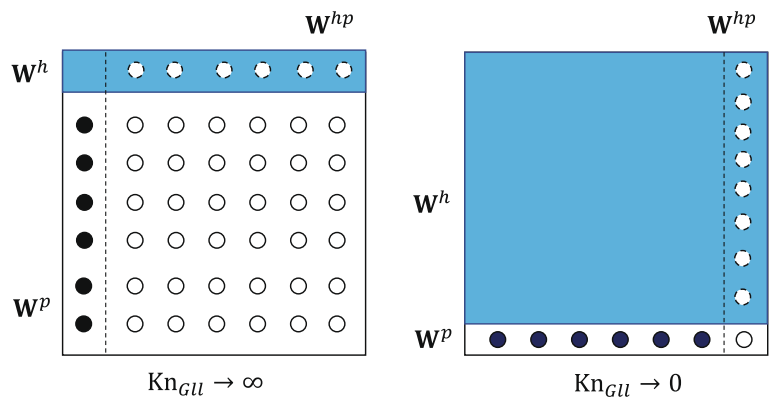

Fig. 4 Illustration for the wave-particle decomposition of the AUGKWP method in the limit of free molecular and continuum flow regimes

flow regimes according to this parameter in the conventional domain-decomposition approaches. In other words, the AUGKWP method has no buffer zones to distinguish and connect fluid and kinetic solvers. Additionally, since the gradient-length local Knudsen number is not influenced by the numerical resolution in a computational domain, it only identifies the local non-equilibrium state. The analytical wave will be mainly used in the equilibrium and near-equilibrium regimes whatever the cell resolution $(\Delta x, \Delta t)$ is adapted in AUGKWP, and the computational efficiency will be improved significantly.

5 Numerical validation

In this section, the AUGKWP method is tested in many cases. Since most of the cases are external flows, the determination of the initial condition of the free stream at different Knudsen numbers will be provided here first. For a specific gas, the density in the free stream corresponding to a given Knudsen number is

$$\rho = \frac{4\alpha(5-2\omega)(7-2\omega)}{5(\alpha+1)(\alpha+2)}\sqrt{\frac{m}{2\pi k_B T}}\frac{\mu}{L_{ref}Kn},$$

where m is the molecular mass and L_{ref} is the reference length to define the Knudsen number. The dynamic viscosity is calculated from the translational temperature by the power law,

$$\mu = \mu_{ref}\left(\frac{T}{T_{ref}}\right)^{\omega},$$

where μ_{ref} is the reference dynamic viscosity at the temperature T_{ref}.

In the tests, a diatomic gas of nitrogen gas is employed with molecular mass $m = 4.65 \times 10^{-26}$ kg, $\alpha = 1.0$, $\omega = 0.74$, and the reference dynamic viscosity $\mu_{ref} = 1.65 \times 10^{-5}$ Nsm^{-2} at the temperature $T_{ref} = 273$ K. In the computations, the freestream or upstream values are used to non-dimensionalize the flow variables, i.e.,

$$\begin{aligned} \rho_0 =& \rho_\infty, \quad U_0 = \sqrt{2k_B T_\infty/m}, \\ T_0 =& T_\infty, \quad \text{or} \quad p_0 = p_\infty. \end{aligned}$$

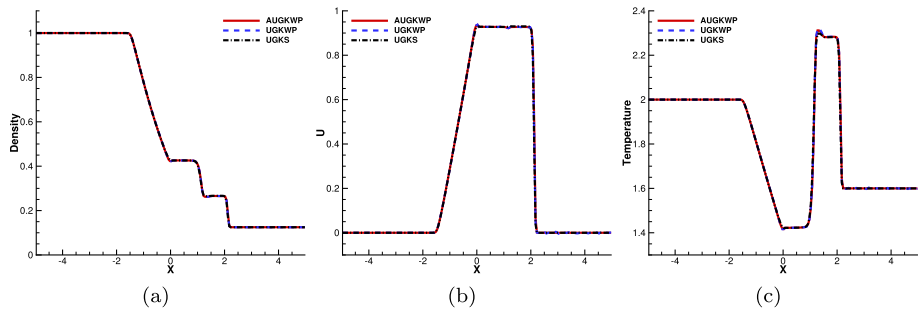

Fig. 5 Sod tube at $Kn = 10^{-5}$. (**a**) Density, (**b**) velocity, and (**c**) temperature

5.1 Sod shock tube test

The Sod shock tube problem is computed at different Knudsen numbers to verify the acceleration effect and capability for simulating the continuum and rarefied flows by the AUGKWP method. The non-dimensional initial condition is

$$(\rho, U, V, W, p) = \begin{cases} (1, 0, 0, 0, 1), & 0 < x < 0.5, \\ (0.125, 0, 0, 0.1), & 0.5 < x < 1. \end{cases}$$

The spatial discretization is carried out by a one-dimensional structured mesh with 200 uniform cells. The inlet and outlet of the tube are treated as far fields. The Courant–Friedrichs–Lewy (CFL) number is taken as 0.5. The critical value for wave-particle decomposition is chosen as $Kn_{ref} = 0.01$. The output time of the simulation is $t = 0.12$.

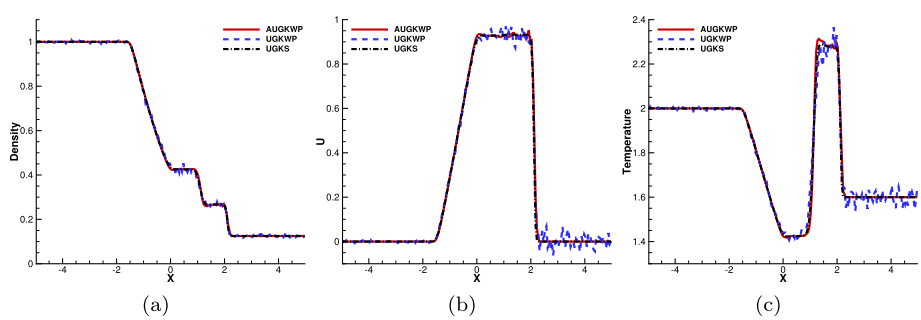

Fig. 6 Sod tube at $Kn = 10^{-4}$. (**a**) Density, (**b**) velocity, and (**c**) temperature

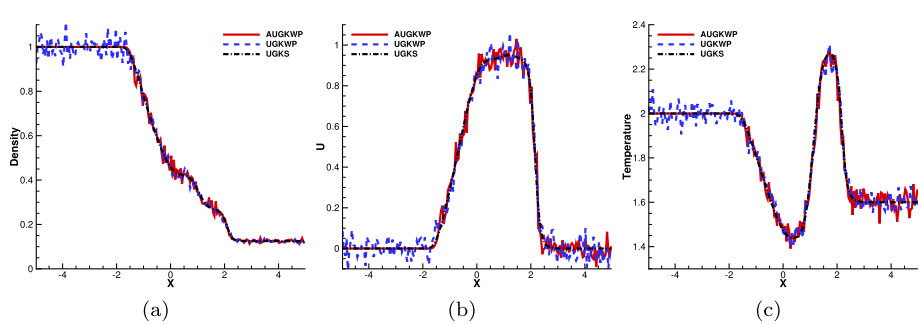

Fig. 7 Sod tube at $Kn = 10^{-3}$. (**a**) Density, (**b**) velocity, and (**c**) temperature

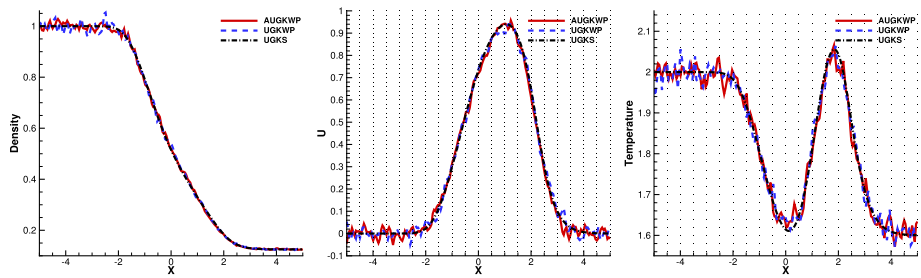

(a) (b) (c)

Fig. 8 Sod tube at $Kn = 10^{-2}$. (**a**) Density, (**b**) velocity, and (**c**) temperature

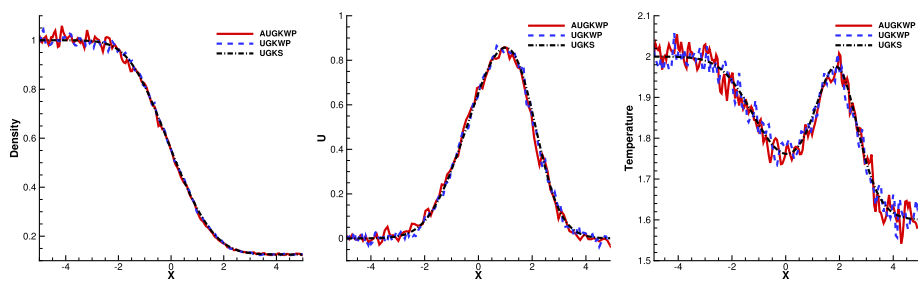

(a) (b) (c)

Fig. 9 Sod tube at $Kn = 10^{-1}$. (**a**) Density, (**b**) velocity, and (**c**) temperature

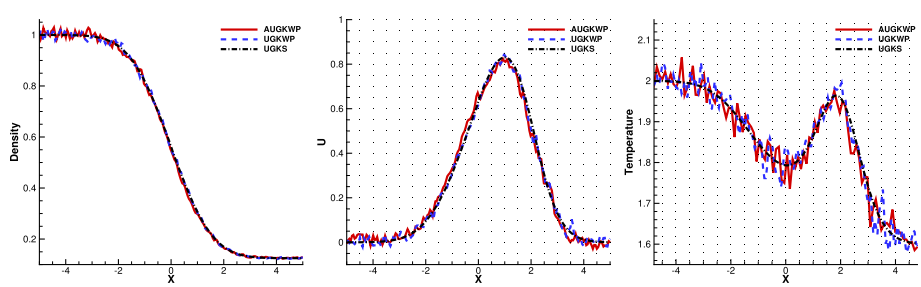

(a) (b) (c)

Fig. 10 Sod tube at $Kn = 1$. (**a**) Density, (**b**) velocity, and (**c**) temperature

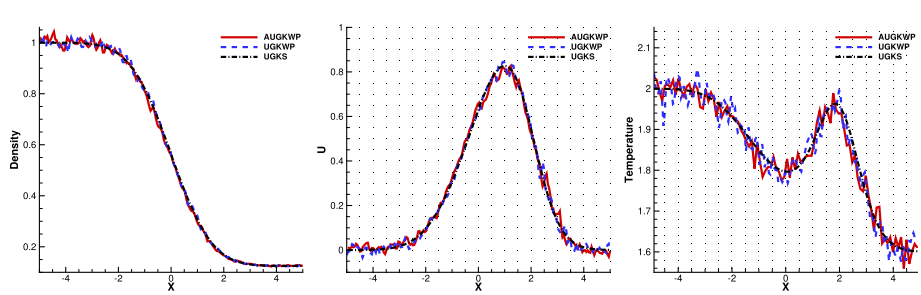

(a) (b) (c)

Fig. 11 Sod tube at $Kn = 10$. (**a**) Density, (**b**) velocity, and (**c**) temperature

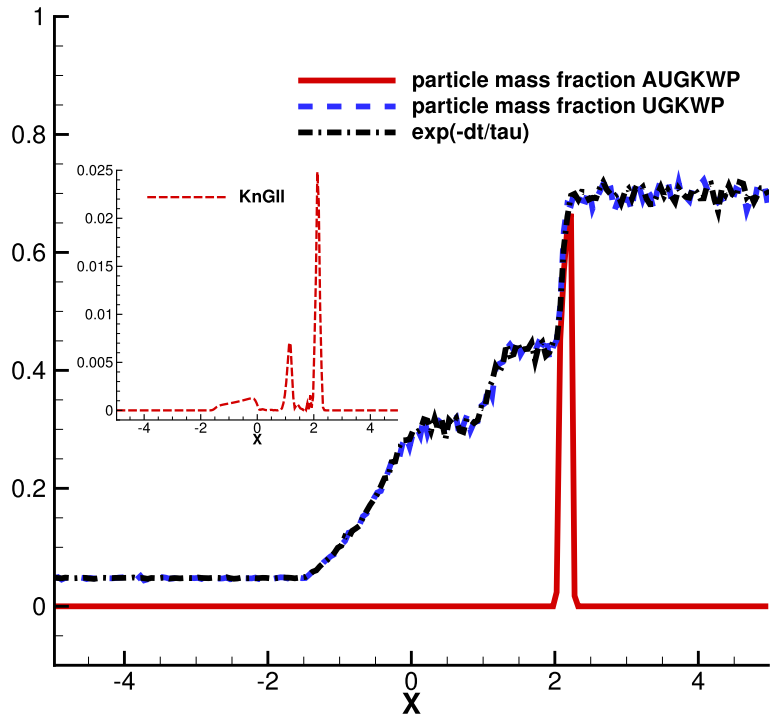

Fig. 12 Numerical particle mass fraction of the original UGKWP method and the AUGKWP method, the exponential function of the cell Knudsen number $e^{-\Delta t/\tau}$, and the gradient-length local Knudsen number Kn_{Gll} for the Sod tube at $Kn = 10^{-4}$

The density, velocity and temperature obtained by the original UGKWP method, the AUGKWP method, and UGKS at different Knudsen numbers from 10^{-5} to 10 are plotted in Figs. 5, 6, 7, 8, 9, 10 and 11. The preset reference number of particles in both the original UGKWP and AUGKWP methods is 400 per cell. Here, the purpose of setting this number of particles in computation is to show that the noise introduced in the AUGKWP method is acceptable compared with the original UGKWP method for unsteady flows when particles are not sufficiently enough. The results show the AUGKWP method can maintain the same solutions as the original UGKWP method and match with the UGKS solutions in all Knudsen regimes.

In these tests, a small time step determined by high spatial resolution leads to a large cell Knudsen number $Kn_c = \tau/\Delta t$. For the original UGKWP method, particles are sampled according to $e^{-\Delta t/\tau}$ for the free transport particle with $t_f = \Delta t$ even in the uniform equilibrium regions. For the AUGKWP method, the analytical wave formulation will be used in the equilibrium region. The numerical particle mass fraction given by the original UGKWP method and the AUGKWP method, the exponential function of the cell Knudsen number $e^{-\Delta t/\tau}$, and the gradient-length local Knudsen number Kn_{Gll} for the Sod tube at $Kn = 10^{-4}$ are plotted in Fig. 12. It shows the particles appear in the original UGKWP method even though the flow regime is continuum, while for the AUGKWP method, with the consideration of the local Knudsen number, particles are sampled in the non-equilibrium region only, such as the shock front region with $Kn_{Gll} > 0.01$. Therefore, high computational efficiency is achieved in AUGKWP. Table 1 is the comparison of the simulation times between the original

Table 1 Comparison of simulation time between the original UGKWP and AUGKWP methods

Knudsen number	Original UGKWP (s)	AUGKWP (s)
10	77.04	70.75
1	78.76	75.05
10^{-1}	82.06	76.37
10^{-2}	98.36	81.12
10^{-3}	124.28	42.89
10^{-4}	164.33	3.45
10^{-5}	181.19	0.41

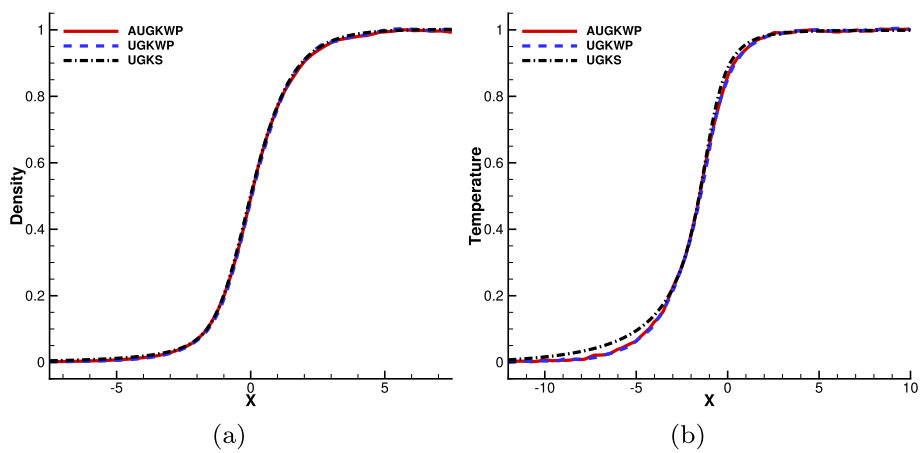

Fig. 13 Shock structure at $Ma = 4$. (**a**) Density and (**b**) temperatures compared with the original UGKWP method and the UGKS. The modification of the particle collision time is not used in UGKS

UGKWP and AUGKWP methods at different Knudsen numbers. It shows the AUGKWP method fully recovers the hydrodynamical solver without using particles in the equilibrium flow regime regardless of the cell resolution used.

5.2 Shock structure

To validate the capability of the AUGKWP method for describing a strong non-equilibrium state, shock structure at upstream Mach number $Ma = 4$ and 10 is investigated. The computational domain $[-25, 25]$ has a length of 50 times of the particle mean free path and is divided by 100 cells uniformly. The left and right boundaries are treated as far field conditions. The CFL number takes 0.5. The reference Knudsen number is $Kn_{ref} = 0.001$. In this study, the upstream temperature is $T_1 = 50$ K. The rest of the parameters could be obtained from the non-dimensional initial condition.

In the kinetic theory, the particle collision time depends on the particle velocity. In order to cope with this physical reality, the relaxation time of the high-speed particles is amended in the UGKWP and AUGKWP methods [53],

$$\tau^* = \begin{cases} \tau, & \text{if } |\boldsymbol{u} - \boldsymbol{U}| \le b\sqrt{RT}, \\ \frac{1}{1+a^*|\boldsymbol{u}-\boldsymbol{U}|/\sqrt{RT}}\tau, & \text{if } |\boldsymbol{u} - \boldsymbol{U}| > b\sqrt{RT}, \end{cases}$$

with two parameters $a = 0.1$ and $b = 5$.

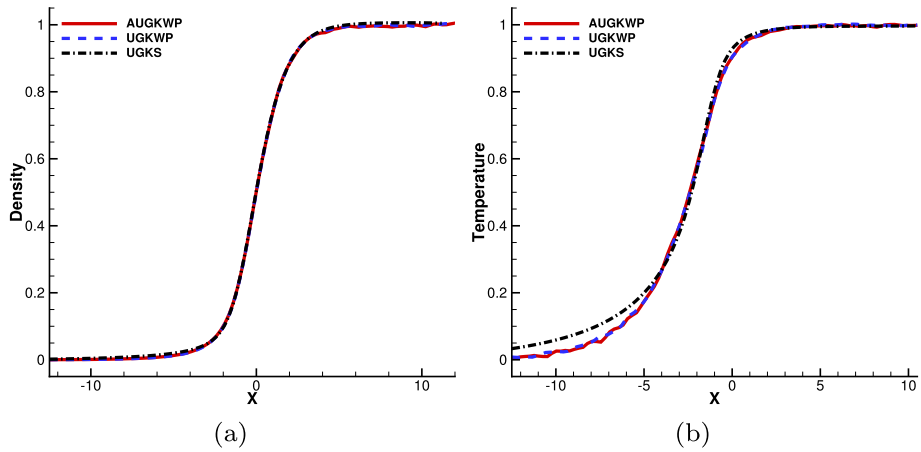

Fig. 14 Shock structure at $Ma = 10$. (**a**) Density and (**b**) temperatures compared with the original UGKWP method and the UGKS. The modification of the particle collision time is not used in UGKS

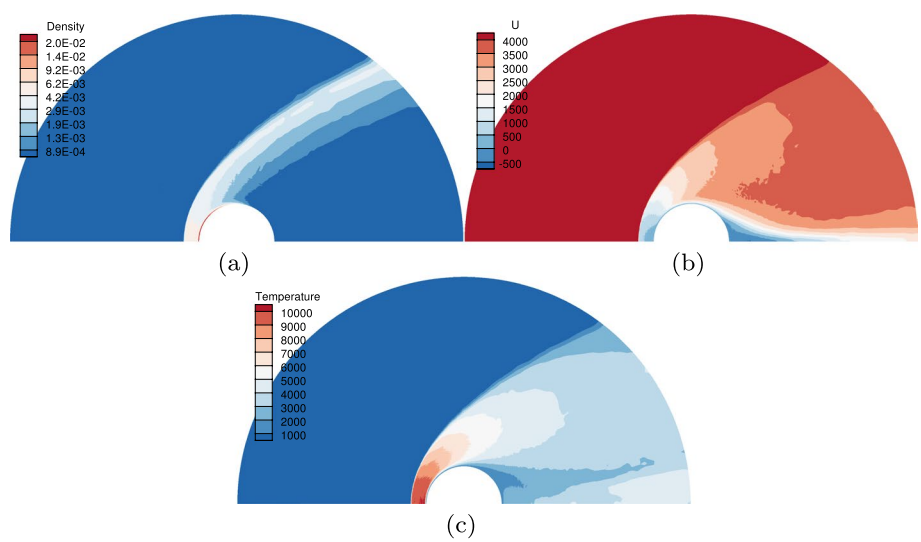

Fig. 15 Hypersonic flow at $Ma = 15$ and $Kn = 0.001$ around a semi-circular cylinder. (**a**) Density, (**b**) x direction velocity, and (**c**) temperature contours

For the UGKWP and AUGKWP methods, 400 simulation particles are used in each cell. To reduce the statistical noise, the time-averaging process is taken from the 2500th step over 12500 steps. The normalized density and temperature from the original UGKWP method, the AUGKWP method, and the UGKS are plotted in Figs. 13–14. The results from the current method have good agreement with that from the original UGKWP method and the deterministic method.

5.3 Flow around a circular cylinder

High-speed flow passing over a semi-circular cylinder at a Mach number of 15 and $Kn = 0.001$ is simulated. The diameter of the cylinder is $D = 0.08$ m. The Knudsen number is defined with respect to the diameter. The computational domain is discretized by $280 \times 200 \times 1$ quadrilateral cells. The initial reference number of particles N_r is set as

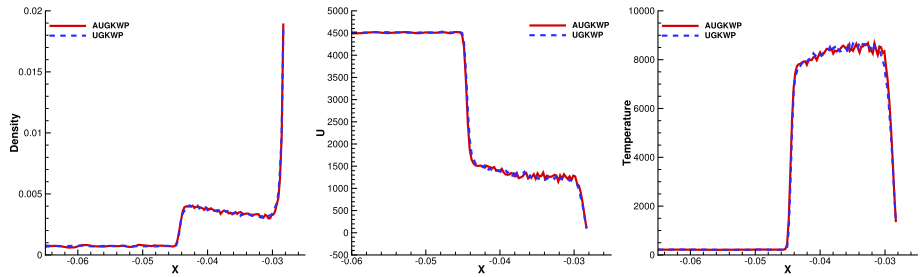

Fig. 16 Hypersonic flow at $Ma = 15$ and $Kn = 0.001$ around a semi-circular cylinder. (**a**) Density, (**b**) x direction velocity, and (**c**) temperature distributions along the 45° extraction line at $Ma = 15$ and $Kn = 0.001$

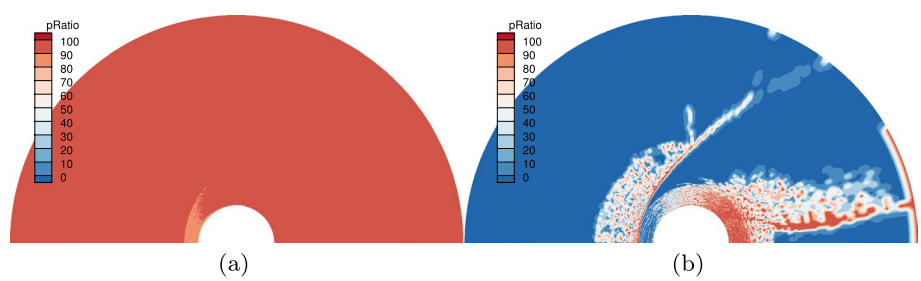

Fig. 17 Hypersonic flow at $Ma = 15$ and $Kn = 0.001$ around a semi-circular cylinder. Numerical particle mass fraction distributions given by (**a**) the original UGKWP method and (**b**) the AUGKWP method

2000. The initial temperature of the free stream gives $T_\infty = 217.5$ K, and the isothermal wall temperature is fixed at $T_w = 1000$ K. The CFL number is 0.5. The reference Knudsen number is $Kn_{ref} = 0.01$. Figure 15 plots the contours of the flow field computed by the AUGKWP method, where an initial flow field provided by 10000 steps of the GKS calculation [51] is adopted, and 60000 steps of the AUGKWP and UGKWP methods have been carried out to achieve a steady state. Figure 16 shows the comparison between the AUGKWP method and the original UGKWP method for the density, velocity in the x direction, and temperature extracted along the 45° line in the upstream. The results from the AUGKWP method are reasonable. The numerical particle mass fraction in Fig. 17 implies the efficiency of the new wave-particle decomposition method. The simulation times for the AUGKWP and UGKWP methods on Tianhe-2 with 3 nodes (72 cores, Intel Xeon E5-2692 v2, 2.2 GHz) are 15623 s and 30487 s, respectively.

5.4 Flow around an Apollo reentry capsule

Hypersonic flow at $Ma = 5$ and $Kn = 10^{-3}$ passing over an Apollo reentry capsule in the transition flow regime is simulated for nitrogen gas. This case shows the efficiency and capability of the AUGKWP method for simulating the large-scale three-dimensional hypersonic flow. The reference length for the definition of the Knudsen number is $L_{ref} = 3.912$ m. As shown in Fig. 18, the mesh consists of 372500 cells. The reference Knudsen number is set as $Kn_{ref} = 0.01$ and the initial reference number of particles N_r is 400 per cell. The flow at free stream has an initial temperature $T_\infty = 142.2$ K, and the

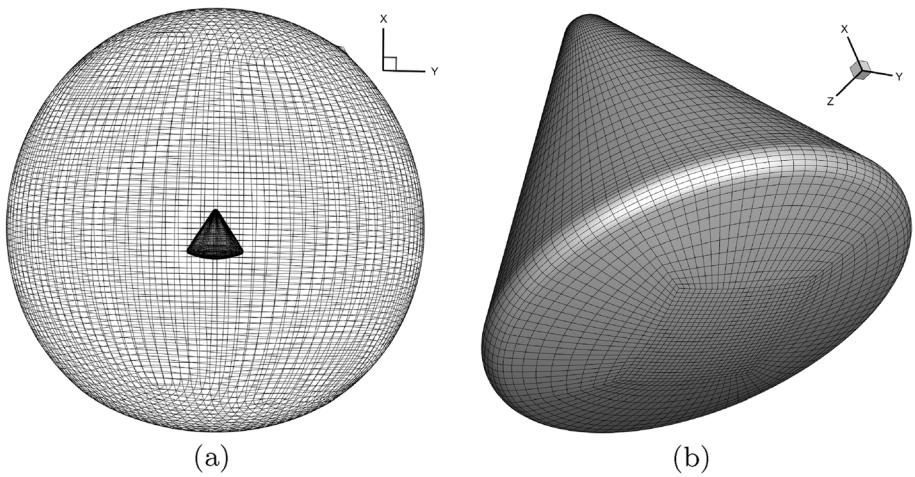

Fig. 18 Mesh of the Apollo reentry capsule. (**a**) Global view and (**b**) local enlargement

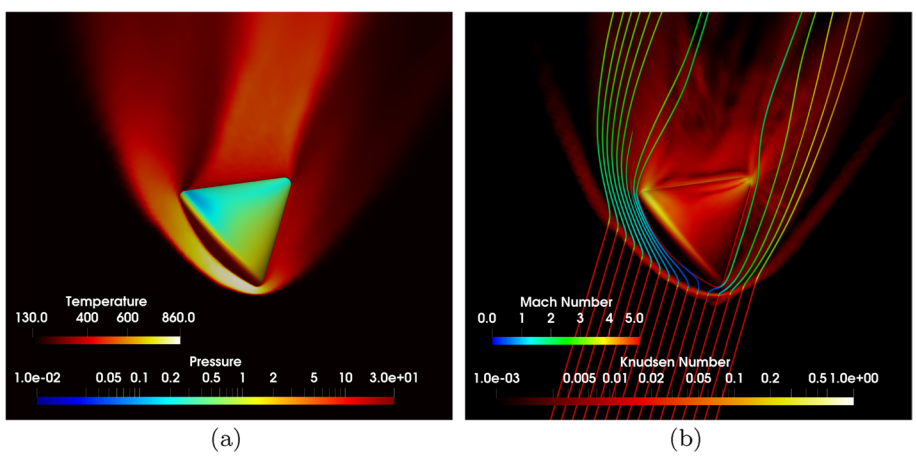

Fig. 19 Hypersonic flow at $Ma = 5$ and $Kn = 0.001$around an Apollo reentry capsule. (**a**) Temperature and pressure distributions, and (**b**) local Knudsen Number Kn_{GII} distribution and Mach number along the streamline

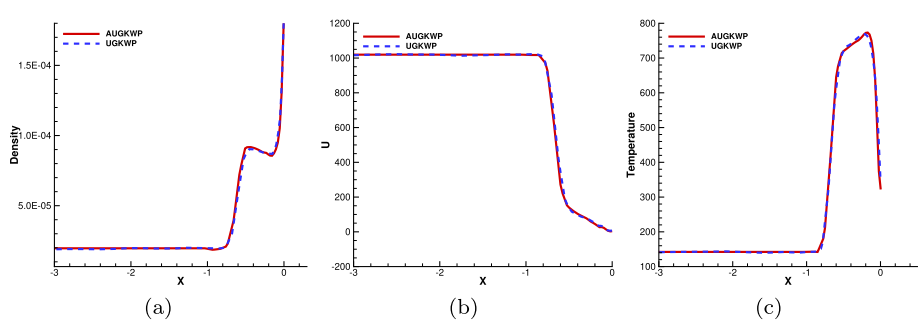

Fig. 20 (**a**) Density, (**b**) x direction velocity, and (**c**) temperature distributions along the windward central axis at $Ma = 5$ and $Kn = 0.001$

reentry surface is treated as an isothermal wall with a constant temperature $T_w = 500$ K. The angle of attack is 30°. The initial flow field is prepared by the GKS calculation with 10000 steps. Then, 25000 steps have been carried out to achieve a steady state solution.

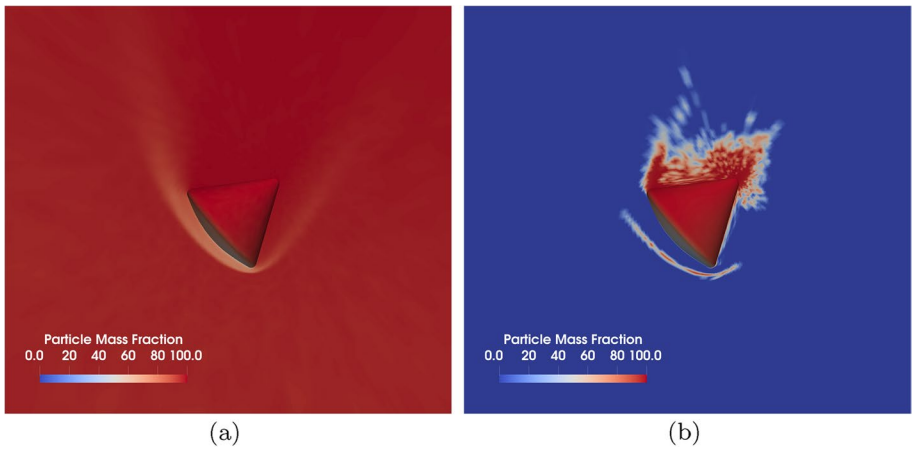

Fig. 21 Hypersonic flow at $Ma = 5$ and $Kn = 0.001$around an Apollo reentry capsule. Numerical particle mass fraction distributions given by (**a**) the original UGKWP method and (**b**) the AUGKWP method

Figure 19 shows the distributions of temperature, pressure, local Knudsen number and Mach number computed by the AUGKWP method. The quantitative comparison between the AUGKWP method and the original UGKWP method for the density, velocity in the x direction, and temperature extracted from the central axis along the windward is plotted in Fig. 20. Good agreement has been obtained. The efficiency of the AUGKWP method has been much improved due to its well controlled mass fraction of particles, as shown in Fig. 21. Particles in the non-equilibrium flow are presented. The computational times for the AUGKWP and UGKWP methods are 24545 s and 42154 s on Tianhe-2 with 5 nodes (120 cores, Intel Xeon E5-2692 v2, 2.2 GHz). The AUGKWP method becomes an indispensable tool for large-scale three-dimensional hypersonic rarefied flow simulations.

5.5 Nozzle plume flow into a background vacuum

In this case, the AUGKWP method is applied to the CO_2 expansions into a background vacuum. The unsteady and multiscale process of this plume flow is hard to compute with acceptive accuracy by conventional DSMC-CFD hybrid methods with time-dependent buffer zones, especially in the initial flow expansion stage. The UGKS, as a multiscale method, is hard to simulate such a flow with the requirement of covering a wide range of discretized particle velocity space to capture the high Mach number jet in the flow acceleration process through the nozzle. The AUGKWP method treats the multiscale and multispeed expansion flow systematically through the dynamically adaptive wave-particle decomposition in each numerical cell, and makes the simulation acceptable in the memory requirement.

The geometry of the nozzle and the two-dimensional mesh with 47186 cells are used in the simulation, as shown in Fig. 22. The inlet boundary condition is set with a temperature 710 K and pressure 36.5 torr. The gas CO_2 is employed with the molecular mass $m = 7.31 \times 10^{-26}$ kg, the ratio of specific heats $\gamma = 1.4$, and $\omega = 0.67$. The nozzle wall is treated as an isothermal one with $T_w = 300$ K. The background environment is set with a temperature $T_B = 300$ K and low pressure $P_B = 0.01$ Pa. The CFL number is 0.5.

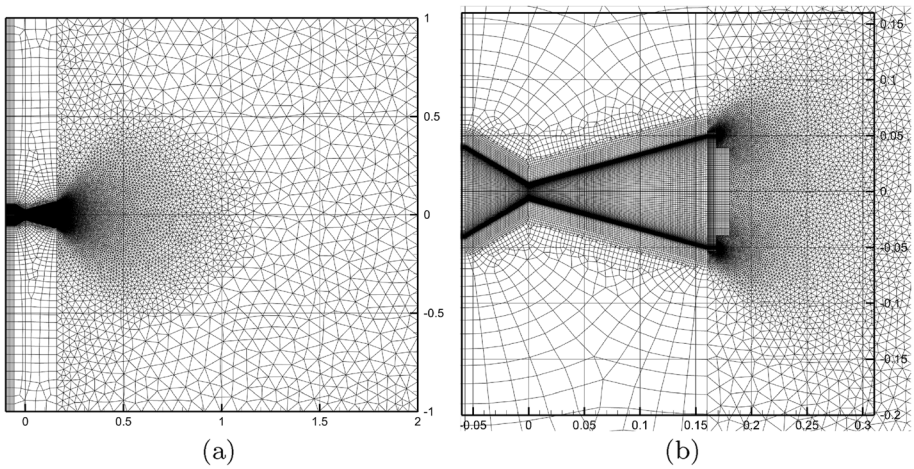

Fig. 22 Mesh of the nozzle. (**a**) Grid used in computation and (**b**) the geometry of the nozzle

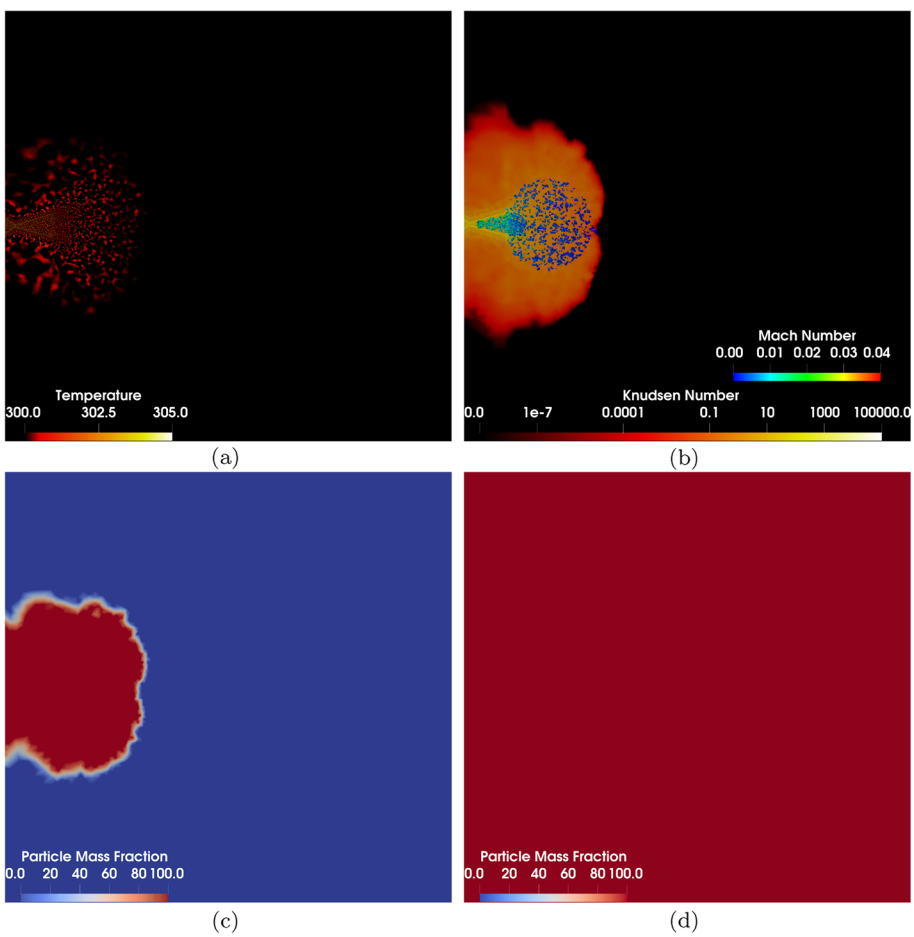

Fig. 23 Nozzle plume flow to a background vacuum at the initial stage. Distributions of (**a**) Temperature, (**b**) local Knudsen number and Mach number along the streamline, (**c**) numerical particle mass fraction of the AUGKWP method, and (**d**) numerical particle mass fraction of the UGKWP method

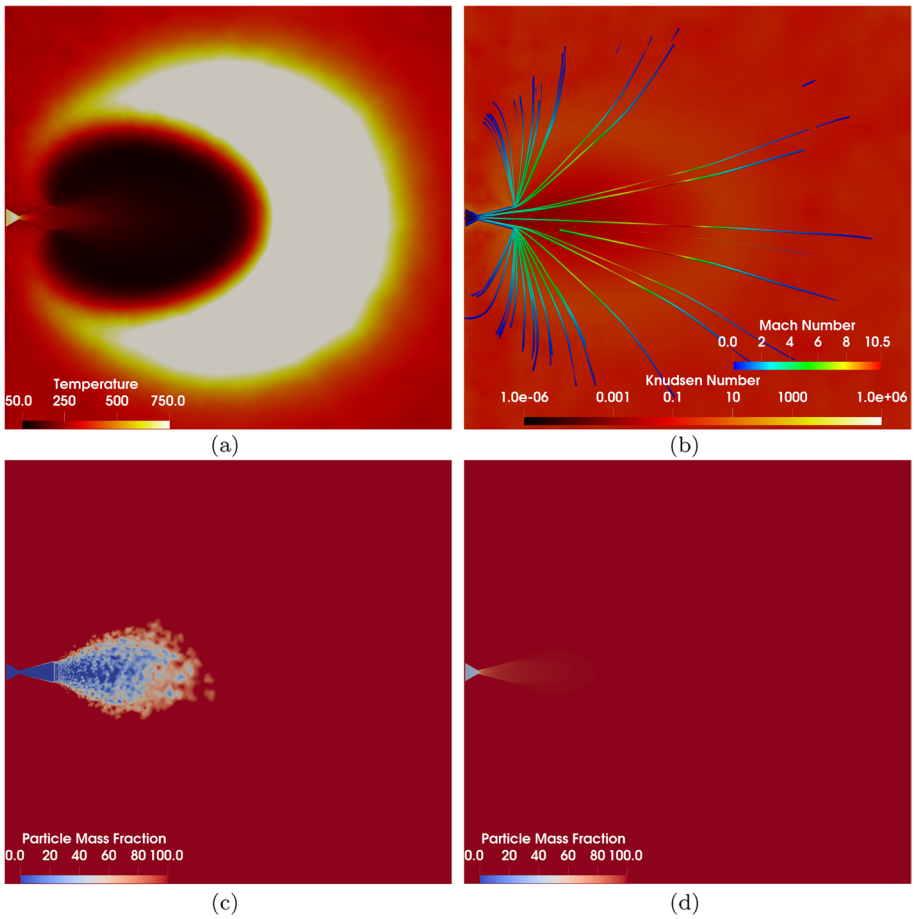

Fig. 24 Nozzle plume flow to a background vacuum at the developing stage. Distributions of (**a**) Temperature, (**b**) local Knudsen number and Mach number along the streamline, (**c**) numerical particle mass fraction of the AUGKWP method, and (**d**) numerical particle mass fraction of the UGKWP method

The reference number of particles is $N_r = 400$. For the AUGKWP method, the reference Knudsen number is $Kn_{ref} = 0.01$.

The simulation covers the whole gas expansion process into a background vacuum through three stages, such as the initial, developing, and steady stages. Figures 23, 24 and 25 show the distributions of temperature, gradient-length dependent local Knudsen number, and Mach number along the streamline, and numerical particle mass fraction of the AUGKWP and UGKWP methods in each stage.

The flow field in the initial stage is shown in Fig. 23. Particles with a large mean free path transport first to the background vacuum. The expansion gas forms a non-equilibrium central region. The AUGKWP method employs particles in this highly expanded region only, while the analytical wave is used in other regions. However, the UGKWP method adapts particles everywhere, even in the uniformly undisturbed background equilibrium region.

In the developing stage (see Fig. 24), a continuum flow regime appears near the nozzle exit, a transition regime forms around the high temperature expansion region, and a free molecular flow remains in the front of the plume. The gradient-length local Knudsen number shows a variation with 12 orders of magnitude in the whole computational

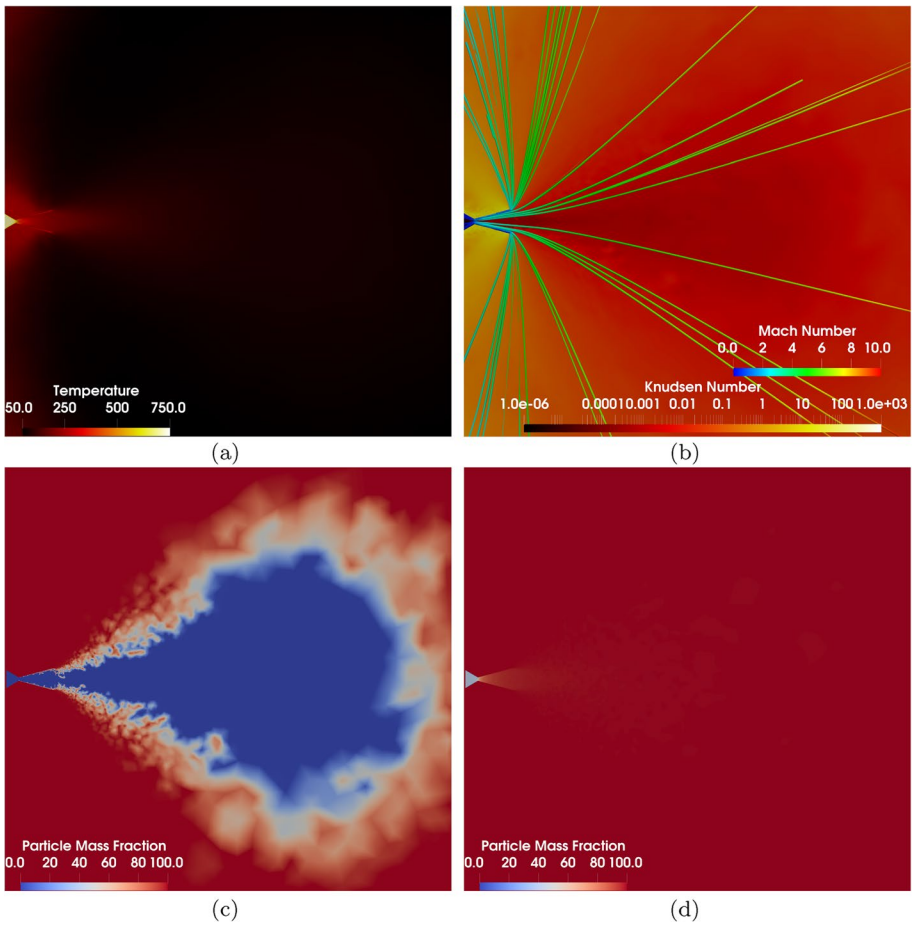

Fig. 25 Nozzle plume flow to a background vacuum at the steady stage. Distributions of (**a**) Temperature, (**b**) local Knudsen number and Mach number along the streamline, (**c**) numerical particle mass fraction of the AUGKWP method, and (**d**) numerical particle mass fraction of the UGKWP method

domain. The simulation of this unsteady multiscale transport requires a method with the capability of capturing continuum and rarefied flows simultaneously at any moment by following the plume flow. The unified treatment in the AUGKWP method with a wave-particle decomposition in each control volume allows an instant and adaptive description in each cell in this expansion process.

Figure 25 presents the plume flow approaching a steady state, where the gas is fully expanded with a steady flow pattern. The AUGKWP method provides a clear separation of different flow regimes, i.e., a continuum flow in the expansion region, a free molecular flow in the background flow, and a transition flow between them (see Fig. 25(c)). In the original UGKWP method, the numerical time step determined by the smallest cell size leads the particle representation in almost the whole computational domain. The quantitative comparison of the density, velocity in the x direction, and temperature along the centerline at the steady stage is plotted in Fig. 26. It shows agreement between the results given by the AUGKWP and UGKWP methods.

Overall, the AUGKWP method gives a non-equilibrium state guided wave-particle decomposition. The computational times in the current studies on Tianhe-2 with 20

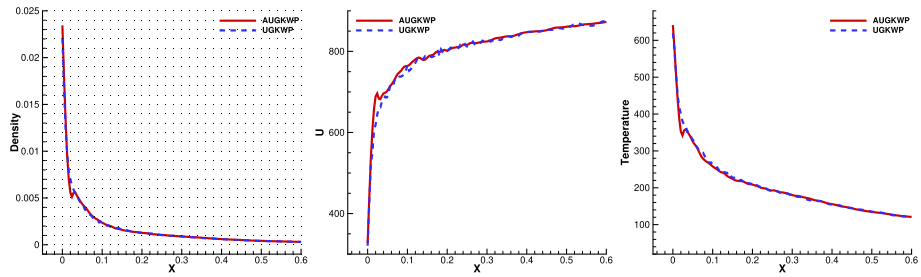

(a) (b) (c)

Fig. 26 Nozzle plume flow to a background vacuum at the steady stage. (**a**) Density, (**b**) *x* direction velocity, and (**c**) temperature from the UGKWP and AUGKWP methods along the centerline

nodes (480 cores) are 12.6 hours and 36.1 hours for the AUGKWP and UGKWP methods, respectively.

6 Conclusion

The UGKWP method is a multiscale method for flow simulations in all regimes. The UGKWP method adopts a wave-particle decomposition to recover the multiscale transport uniformly in each control volume. In this paper, an adaptive unified gas-kinetic wave-particle (AUGKWP) method is developed to further optimize the wave-particle decomposition in the original UGKWP. In order to concentrate particles in the non-equilibrium region only, instead of using the cell Knudsen number $Kn_c = \tau/\Delta t$ only in the original UGKWP method, the AUGKWP method introduces a flow gradient-related local Knudsen number as well for the decomposition of wave and particle. As a result, the AUGKWP method avoids using particles in the highly dilute background equilibrium region and in the continuum flow simulation with the use of an extremely small numerical time step. The AUGKWP method provides a physically reliable wave-particle decomposition and guarantees the appearance of particles in the non-equilibrium region only, regardless of the mesh resolution. Many test cases are used to validate the efficiency and accuracy of the AUGKWP method. In comparison with the original UGKWP method, due to the significant reduction of particles in the AUGKWP method, the scheme can speed up the computation, reduce the memory requirement, and maintain the same solution accuracy as the original multiscale wave-particle method. The AUGKWP method will become a useful and indispensable tool in the simulation of high-speed rarefied and continuum flows in aerodynamic applications.

Acknowledgements
The CFD group members at HKUST are deserving of the authors' gratitude for their weekly discussions and collaborative efforts.

Authors' contributions
All authors contributed equally to this work.

Funding
This work was supported by the National Key R&D Program of China (Grant No. 2022YFA1004500), National Natural Science Foundation of China (Grant No. 12172316), and the Hong Kong Research Grants Council (Grant Nos. 16208021, 16301222).

Availability of data and materials
The data that support the findings of this study are available from the corresponding author upon reasonable request.

Declarations

Competing interests
Not applicable.

Received: 3 April 2023 Accepted: 23 July 2023
Published online: 03 October 2023

References

1. Bird GA (1994) Molecular gas dynamics and the direct simulation of gas flows, 2nd edn. Clarendon Press, Oxford
2. Xu K (2021) A unified computational fluid dynamics framework from rarefied to continuum regimes. Cambridge University Press, Oxford
3. Fan J, Shen C (2001) Statistical simulation of low-speed rarefied gas flows. J Comput Phys 167(2):393–412
4. Shen C (2005) Rarefied gas dynamics: fundamentals, simulations and micro flows. Springer Berlin, Heidelberg
5. Sun Q, Boyd ID (2002) A direct simulation method for subsonic, microscale gas flows. J Comput Phys 179(2):400–425
6. Baker LL, Hadjiconstantinou NG (2005) Variance reduction for Monte Carlo solutions of the Boltzmann equation. Phys Fluids 17(5):051703
7. Homolle TM, Hadjiconstantinou NG (2007) A low-variance deviational simulation Monte Carlo for the Boltzmann equation. J Comput Phys 226(2):2341–2358
8. Degond P, Dimarco G, Pareschi L (2011) The moment-guided Monte Carlo method. Int J Numer Methods Fluids 67(2):189–213
9. Pareschi L, Russo G (2000) Asymptotic preserving Monte Carlo methods for the Boltzmann equation. Transp Theory Stat Phys 29(3–5):415–430
10. Ren W, Liu H, Jin S (2014) An asymptotic-preserving Monte Carlo method for the Boltzmann equation. J Comput Phys 276:380–404
11. Dimarco G, Pareschi L (2011) Exponential Runge-Kutta methods for stiff kinetic equations. SIAM J Numer Anal 49(5):2057–2077
12. Chu CK (1965) Kinetic-theoretic description of the formation of a shock wave. Phys Fluids 8(1):12–22
13. Yang JY, Huang JC (1995) Rarefied flow computations using nonlinear model Boltzmann equations. J Comput Phys 120(2):323–339
14. Mieussens L (2000) Discrete-velocity models and numerical schemes for the Boltzmann-BGK equation in plane and axisymmetric geometries. J Comput Phys 162(2):429–466
15. Tcheremissine F (2005) Direct numerical solution of the Boltzmann equation. AIP Conf Proc 762(1):677–685
16. Kolobov VI, Arslanbekov RR, Aristov VV et al (2007) Unified solver for rarefied and continuum flows with adaptive mesh and algorithm refinement. J Comput Phys 223(2):589–608
17. Li Z, Zhang H (2009) Gas-kinetic numerical studies of three-dimensional complex flows on spacecraft re-entry. J Comput Phys 228(4):1116–1138
18. Xu K, Huang J (2010) A unified gas-kinetic scheme for continuum and rarefied flows. J Comput Phys 229(20):7747–7764
19. Wu L, Zhang J, Reese JM et al (2015) A fast spectral method for the Boltzmann equation for monatomic gas mixtures. J Comput Phys 298:602–621
20. Aristov VV (2001) Direct methods for solving the Boltzmann equation and study of nonequilibrium flows. Springer, Dordrecht
21. Li Z, Zhang H (2004) Study on gas kinetic unified algorithm for flows from rarefied transition to continuum. J Comput Phys 193(2):708–738
22. Li Z, Peng A, Ma Q et al (2019) Gas-kinetic unified algorithm for computable modeling of Boltzmann equation and application to aerothermodynamics for falling disintegration of uncontrolled Tiangong-No. 1 spacecraft. Adv Aerodyn 1(1):4
23. Guo Z, Xu K, Wang R (2013) Discrete unified gas kinetic scheme for all Knudsen number flows: Low-speed isothermal case. Phys Rev E 88(3):033305
24. Chen S, Zhang C, Zhu L et al (2017) A unified implicit scheme for kinetic model equations. Part I. Memory reduction technique. Sci Bull 62(2):119–129
25. Chen S, Xu K (2015) A comparative study of an asymptotic preserving scheme and unified gas-kinetic scheme in continuum flow limit. J Comput Phys 288:52–65
26. Zhu Y, Zhong C, Xu K (2016) Implicit unified gas-kinetic scheme for steady state solutions in all flow regimes. J Comput Phys 315:16–38
27. Zhu Y, Zhong C, Xu K (2017) Unified gas-kinetic scheme with multigrid convergence for rarefied flow study. Phys Fluids 29(9):096102
28. Zhu Y, Zhong C, Xu K (2019) An implicit unified gas-kinetic scheme for unsteady flow in all Knudsen regimes. J Comput Phys 386:190–217
29. Jiang D, Mao M, Li J et al (2019) An implicit parallel UGKS solver for flows covering various regimes. Adv Aerodyn 1(1):8
30. Chen S, Xu K, Lee C et al (2012) A unified gas kinetic scheme with moving mesh and velocity space adaptation. J Comput Phys 231(20):6643–6664
31. Mouhot C, Pareschi L (2006) Fast algorithms for computing the Boltzmann collision operator. Math Comput 75(256):1833–1852
32. Wu L, White C, Scanlon TJ et al (2013) Deterministic numerical solutions of the Boltzmann equation using the fast spectral method. J Comput Phys 250:27–52

33. Filbet F, Jin S (2010) A class of asymptotic-preserving schemes for kinetic equations and related problems with stiff sources. J Comput Phys 229(20):7625–7648
34. Dimarco G, Pareschi L (2013) Asymptotic preserving implicit-explicit Runge-Kutta methods for nonlinear kinetic equations. SIAM J Numer Anal 51(2):1064–1087
35. Guo Z, Li J, Xu K (2023) Unified preserving properties of kinetic schemes. Phys Rev E 107(2):025301
36. Li Z, Fang M, Jiang X et al (2013) Convergence proof of the DSMC method and the gas-kinetic unified algorithm for the Boltzmann equation. Sci China Phys Mech Astron 56:404–417
37. Guo Z, Xu K (2021) Progress of discrete unified gas-kinetic scheme for multiscale flows. Adv Aerodyn 3(1):6
38. Fei F, Zhang J, Li J et al (2020) A unified stochastic particle Bhatnagar-Gross-Krook method for multiscale gas flows. J Comput Phys 400:108972
39. Fei F, Ma Y, Wu J et al (2021) An efficient algorithm of the unified stochastic particle Bhatnagar-Gross-Krook method for the simulation of multi-scale gas flows. Adv Aerodyn 3(1):18
40. Liu C, Zhu Y, Xu K (2020) Unified gas-kinetic wave-particle methods I: Continuum and rarefied gas flow. J Comput Phys 401:108977
41. Zhu Y, Liu C, Zhong C et al (2019) Unified gas-kinetic wave-particle methods. II. Multiscale simulation on unstructured mesh. Phys Fluids 31(6):067105
42. Xu K (2015) Direct modeling for computational fluid dynamics: Construction and application of unified gas-kinetic scheme. World Scientific, Hong Kong
43. Liu S, Zhong C, Fang M (2020) Simplified unified wave-particle method with quantified model-competition mechanism for numerical calculation of multiscale flows. Phys Rev E 102(1):013304
44. Yang LM, Li ZH, Shu C et al (2022) Discrete unified gas-kinetic wave-particle method for flows in all flow regimes. Phys Rev E 108(1):015302
45. Xu X, Chen Y, Liu C et al (2021) Unified gas-kinetic wave-particle methods V: Diatomic molecular flow. J Comput Phys 442:110496
46. Wei Y, Zhu Y, Xu K (2022) Unified gas-kinetic wave-particle methods VII: Diatomic gas with rotational and vibrational nonequilibrium. arXiv preprint arXiv:2211.12922
47. Li W, Liu C, Zhu Y et al (2020) Unified gas-kinetic wave-particle methods III: Multiscale photon transport. J Comput Phys 408:109280
48. Liu C, Xu K (2021) Unified gas-kinetic wave-particle methods IV: Multi-species gas mixture and plasma transport. Adv Aerodyn 3(1):9
49. Yang X, Wei Y, Shyy W et al (2022) Unified gas-kinetic wave-particle method for three-dimensional simulation of gas-particle fluidized bed. Chem Eng J 453:139541
50. Bhatnagar PL, Gross EP, Krook M (1954) A model for collision processes in gases. I. Small amplitude processes in charged and neutral one-component systems. Phys Rev 94(3):511–525
51. Xu K (2001) A gas-kinetic BGK scheme for the Navier-Stokes equations and its connection with artificial dissipation and Godunov method. J Comput Phys 171(1):289–335
52. Venkatakrishnan V (1995) Convergence to steady state solutions of the Euler equations on unstructured grids with limiters. J Comput Phys 118(1):120–130
53. Xu X, Chen Y, Xu K (2021) Modeling and computation for non-equilibrium gas dynamics: Beyond single relaxation time kinetic models. Phys Fluids 33(1):011703

Publisher's Note

Springer Nature remains neutral with regard to jurisdictional claims in published maps and institutional affiliations.

Submit your manuscript to a SpringerOpen journal and benefit from:

- ► Convenient online submission
- ► Rigorous peer review
- ► Open access: articles freely available online
- ► High visibility within the field
- ► Retaining the copyright to your article

Submit your next manuscript at ► springeropen.com